

## Effects of growth temperature on the structural and optical properties of 1.55 $\mu\text{m}$ GaInNAsSb quantum wells grown on GaAs

Seth R. Bank,<sup>a)</sup> Homan B. Yuen, Mark A. Wistey, Vincenzo Lordi, Hopil P. Bae, and James S. Harris, Jr.

*Solid State and Photonics Laboratory, Stanford University, Stanford, California 94305*

(Received 1 March 2005; accepted 7 June 2005; published online 8 July 2005)

We investigate the effects of growth temperature on the structural and optical properties of GaInNAsSb single quantum wells grown by molecular beam epitaxy. Peak room-temperature photoluminescence occurred at 1.65  $\mu\text{m}$  as-grown and at 1.55  $\mu\text{m}$  under optimal annealing conditions. Excellent room-temperature optical efficiency was observed from samples grown between 420 and 460  $^{\circ}\text{C}$ , with a maximum at 440  $^{\circ}\text{C}$ . However, luminescence was degraded approximately two orders of magnitude for a sample grown at 470  $^{\circ}\text{C}$ . High-resolution x-ray diffraction showed substantial structural degradation and a reduction in strain for the 470  $^{\circ}\text{C}$  sample. Low temperature photoluminescence measurements were also employed to study localization and quenching effects; both became more severe with increasing growth temperature. © 2005 American Institute of Physics. [DOI: 10.1063/1.1993772]

Recent improvements in the growth of GaInNAs(Sb) alloys on GaAs (Ref. 1) have led to impressive laser results throughout the 1.2–1.6  $\mu\text{m}$  range.<sup>2–6</sup> The favorable band offsets,<sup>1</sup> high quantum well (QW) gain, and the availability of high index contrast GaAs/AlAs distributed mirrors make GaInNAs(Sb) promising for laser applications over this emission range and beyond. Moreover, the relatively large electron effective mass and strong excitonic behavior at room temperature make the dilute-nitrides similarly appealing for modulators<sup>7</sup> and detectors. The addition of small quantities of antimony redshifts emission and dramatically improves the optical quality, as measured by photoluminescence (PL) and laser performance. The key materials challenge that remains for obtaining high-performance devices at long wavelengths ( $>1.5 \mu\text{m}$ ) is the optimization of growth parameters to compensate for the increased nitrogen content that is required.<sup>4–6</sup>

Samples were grown on (100) semi-insulating GaAs substrates by solid-source molecular beam epitaxy, with reactive nitrogen supplied from a rf plasma cell (SVT Associates). The active region was a single 80  $\text{\AA}$  Ga<sub>0.59</sub>In<sub>0.41</sub>N<sub>0.028</sub>As<sub>0.942</sub>Sb<sub>0.03</sub> QW surrounded on either side by 200  $\text{\AA}$  GaN<sub>0.03</sub>As<sub>0.97</sub> strain-compensating barriers. The active layer was grown on a 3000  $\text{\AA}$  GaAs buffer and capped with 500  $\text{\AA}$  of GaAs, both grown at 580  $^{\circ}\text{C}$ . Other details related to the growth techniques are provided elsewhere.<sup>4,5</sup> The active region growth temperature was varied from 420 to 470  $^{\circ}\text{C}$  and monitored with band-edge reflection spectroscopy and pyrometry. Samples were grown out of order (440, 420, 470, 460  $^{\circ}\text{C}$ ) to rule out flux variations as a cause for the observed behavior. Annealing was performed in a rapid thermal annealing (RTA) furnace and arsenic outdiffusion was minimized with a GaAs proximity cap. Photoluminescence measurements were performed using a multiline Ar<sup>+</sup> laser as the excitation source. Luminescence was collected and focused into a grating spectrometer, with slits set for a wavelength resolution of  $\pm 0.5 \text{ nm}$  (unless otherwise speci-

fied). The signal was detected with an uncooled InGaAs photodiode and a lock-in amplifier. Spectra were corrected for the wavelength response of the measurement system. For temperature-dependent PL measurements, as-grown samples were mounted strain-free on the cold finger of a liquid helium cryostat with minimum temperature of 10 K.

Peak room-temperature PL emission occurred at  $\sim 1.65 \mu\text{m}$  as-grown and at  $\sim 1.55 \mu\text{m}$  under optimal annealing conditions. Figure 1 plots the peak PL intensity as a function of the RTA temperature, for 1 min anneals. Excellent optical efficiency was observed from samples grown between 420 and 460  $^{\circ}\text{C}$ . However, luminescence was strongly degraded for the sample grown at 470  $^{\circ}\text{C}$ . Degradation of optical quality at elevated growth temperatures has also been observed for GaInNAs with high nitrogen content<sup>6</sup> and GaNAs(Sb).<sup>8</sup>

The 420  $^{\circ}\text{C}$  sample showed the highest PL efficiency as grown, but this did not persist upon anneal. Under optimal annealing conditions ( $\sim 740 \text{ }^{\circ}\text{C}$ , for 1 min), the 440  $^{\circ}\text{C}$

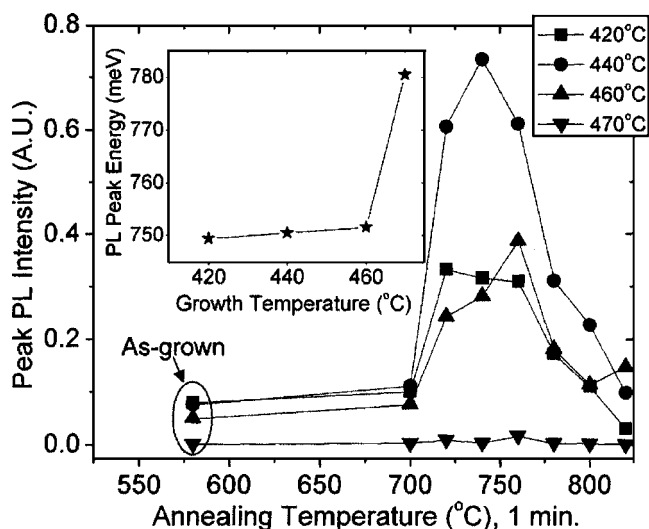


FIG. 1. Peak PL intensity, as a function of postgrowth annealing temperature. Inset shows the peak emission energy (as-grown) at room temperature.

<sup>a)</sup>Electronic mail: sbank@stanfordalumini.org.

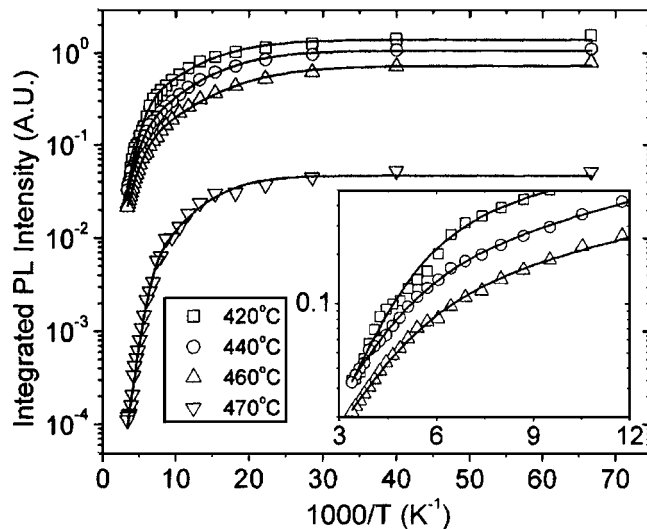


FIG. 2. Integrated PL intensity with temperature. Solid lines are fits to data using the dual activation energy model (see Ref. 9). Inset shows the high temperature data for the 420–460 °C samples.

sample showed  $\sim 2\times$  higher PL signal than those grown at 420 or 460 °C. This indicates the preferential formation of defects at lower growth temperatures that are more resistant to anneal. As shown in the inset of Fig. 1, a slight linear blueshift in the peak emission ( $\sim 1.5$  meV/20 °C) was observed with increasing growth temperature for the samples grown between 420 and 460 °C, likely due to changes in the incorporation kinetics. The 470 °C sample was dramatically blueshifted relative to the other samples, by  $\sim 30$  meV. Differences in the emission energy between samples persisted upon anneal.

The dramatically reduced room-temperature PL efficiency at high growth temperatures is explained, in part, by stronger luminescence quenching effects. Figure 2 plots the integrated luminescence as a function of temperature. Fits to the data with the standard model of two activation energies<sup>9</sup> are also shown. Very similar behavior was observed among the 420–460 °C samples. However, the 470 °C sample showed more than tenfold higher PL quenching with temperature, indicating substantially stronger nonradiative channels. It is also noted that the 420 °C sample showed slightly elevated quenching near room temperature, as compared to the 440 and 460 °C samples (inset of Fig. 2), possibly due to an additional nonradiative path. The 440 °C sample showed the weakest quenching.

High-resolution x-ray diffraction (HR-XRD)  $\omega/2\theta$  (004) measurements of the samples are shown in Fig. 3. Comparable structural quality was observed for samples grown between 420 and 460 °C; however, the sample grown at 470 °C showed a significant reduction in strain for both the QW and GaNAs barriers, possibly due to strain relaxation or microscopic phase segregation. Relaxation may be ruled out as it would redshift the emission. Pendellösung fringe periodicity for the QW peak was dramatically altered as well. Simulations indicate that this was caused by a loss of interface quality between the top GaNAs layer and the GaAs cap. Though not shown, (224) reciprocal space maps showed no relaxation and little difference amongst the samples, aside from a slight broadening of the GaNAs-related features for the 470 °C sample. This broadening may be related to phase segregation and the loss of interface quality.

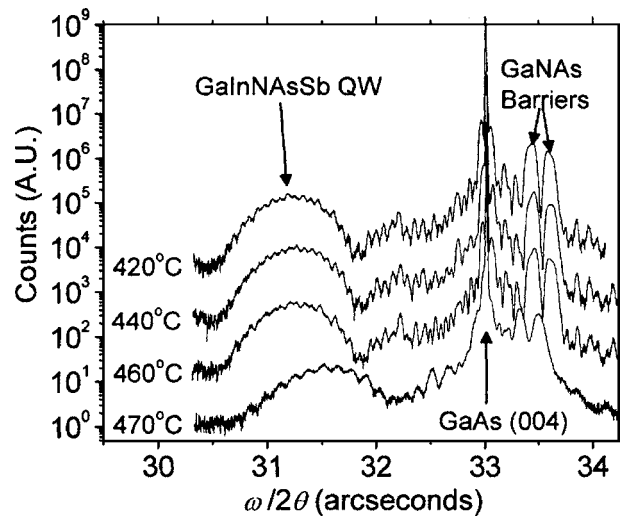


FIG. 3. HR-XRD  $\omega/2\theta$  scans for the different growth temperatures.

To further investigate the growth temperature dependence of the optical properties, low-temperature PL measurements were performed on the as-grown samples. The shift in the PL peak energy with temperature is an ideal method to explore the compositional inhomogeneity that likely results from growth at elevated temperatures.<sup>10–13</sup> Localization effects have been observed in many material systems, including quantum dots, III-nitrides, II–VI alloys, arsenide-phosphides, and the dilute-nitrides. In the presence of potential fluctuations, excitons can become trapped in deep fluctuations unless sufficient thermal energy is present. In the dilute-nitrides, at low temperatures, excitons cannot surmount the small energy barriers and are trapped in local fluctuations. As the temperature is increased, excitons can overcome these barriers and fall into the deepest fluctuations. With greater thermal energy, some carriers may escape even the deep fluctuations, causing delocalized emission to dominate due to its greater optical efficiency. The luminescence spectrum then follows the traditional Varshni behavior with temperature. This leads to a redshift-blueshift-redshift behavior of the peak PL energy with temperature, referred to as an S shape.<sup>10–13</sup> Such effects are easily bleached out, likely due to substantial differences in the relative optical efficiency of the different fluctuations, and are best observed at low excitation densities.

Figure 4 shows the peak PL shift with temperature for the different as-grown samples. Qualitatively, the peaks shifted similarly; however, differences were quite clear at low temperatures (inset of Fig. 4). An initial blueshift with increasing measurement temperature was observed for the 440–470 °C samples, at an excitation density of 100 W/cm<sup>2</sup>, with the degree of blueshift generally increasing with growth temperature. By contrast, the 420 °C sample showed no blueshift, indicating that delocalized emission dominates even at low temperatures. Under a substantially lower excitation density of 1 W/cm<sup>2</sup>, localization effects were even more pronounced, as shown in Fig. 5 for the 440 and 470 °C samples. The 440 °C sample showed a more substantial blueshift with temperature,  $\sim 3$  meV, while the 470 °C exhibited a clear S shape with a depth of  $\sim 12$  meV. This clearly indicates that compositional fluctuations and, hence, localization become more severe with increasing growth temperature.

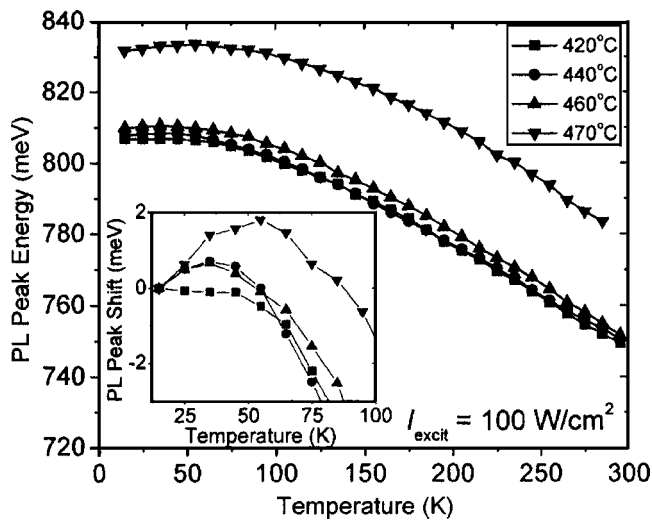


FIG. 4. Peak PL energy with temperature for the different growth temperatures, taken under  $100 \text{ W/cm}^2$  excitation. Inset shows the peak shift for low temperatures. The peak uncertainty was  $\pm 0.25 \text{ meV}$ .

Such effects were also observed in the low-temperature PL lineshape. Figure 6 plots the PL spectra at 25 K for the different growth temperatures, at an excitation of  $10 \text{ W/cm}^2$ . Band tailing effects are evident from a comparison of the  $470^\circ\text{C}$  sample with those grown at lower temperatures. The luminescence line shape reflects the energy distribution of band tail states, causing a pronounced low-energy tail. This has been observed in several materials, including GaNAs (Ref. 10) and GaAsP.<sup>14</sup> Following the work of Buyanova *et al.*,<sup>10</sup> fitting the low-energy tail to an exponential decay allows for an estimate of the localization potential of the fluctuations. The localization potential for the structures grown between  $420$  and  $460^\circ\text{C}$  was  $\sim 6\text{--}7 \text{ meV}$ , but increased to  $\sim 17 \text{ meV}$  for the  $470^\circ\text{C}$  sample.

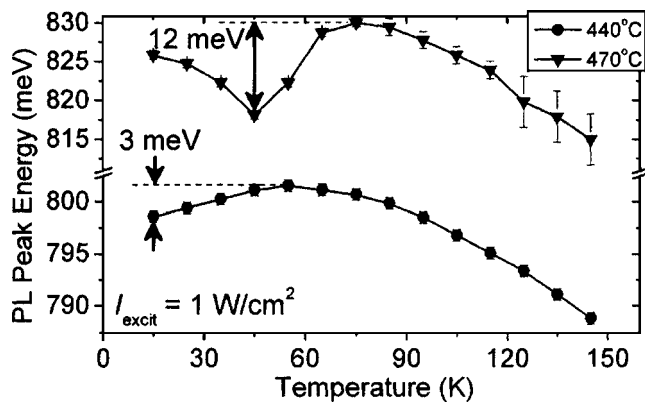


FIG. 5. Peak PL shift with temperature under a reduced excitation density of  $1 \text{ W/cm}^2$ . Localization effects were considerably more pronounced, including a clear S shape for the  $470^\circ\text{C}$  sample.

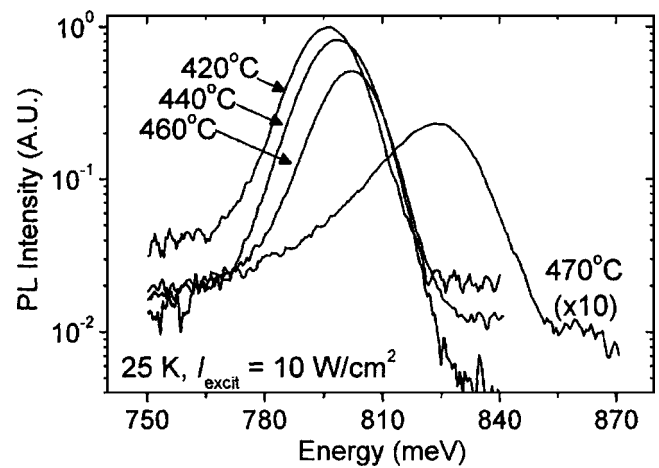


FIG. 6. PL spectra at 25 K for the different growth temperature samples.

In conclusion, we have investigated high-quality GaInNAsSb QWs, grown on GaAs, with emission  $\sim 1.55 \mu\text{m}$  after anneal. Measurements indicate that high-efficiency material may be grown over a reasonably wide temperature range, but a critical maximum temperature does exist. Localization and PL quenching effects were substantially increased at higher growth temperature; however, samples grown below the critical point behaved quite similarly.

This work was supported under DARPA, ARO, the MARCO Interconnect Focus Center, and the Stanford Network Research Center (SNRC). The authors thank Luxtron for the pyrometer used in this study. V.L. was supported by the Hertz Foundation.

- <sup>1</sup>M. Kondow, K. Uomi, A. Niwa, T. Kitatani, S. Watahiki, and Y. Yazawa, *Jpn. J. Appl. Phys., Part 1* **35**, 1273 (1996).
- <sup>2</sup>D. A. Livshits, A. Yu Egorov, and H. Riechert, *Electron. Lett.* **36**, 1381 (2000).
- <sup>3</sup>N. Tansu and L. J. Mawst, *IEEE Photonics Technol. Lett.* **14**, 444 (2002).
- <sup>4</sup>S. R. Bank, M. A. Wistey, H. B. Yuen, L. L. Goddard, W. Ha, and J. S. Harris, Jr., *Electron. Lett.* **39**, 1445 (2003).
- <sup>5</sup>S. R. Bank, M. A. Wistey, L. L. Goddard, H. B. Yuen, V. Lordi, and J. S. Harris, Jr., *IEEE J. Quantum Electron.* **40**, 656 (2004).
- <sup>6</sup>G. Jaschke, R. Averbek, L. Geelhaar, and H. Riechert, *J. Cryst. Growth* **278**, 224 (2005).
- <sup>7</sup>V. Lordi, H. B. Yuen, S. R. Bank, and J. S. Harris, *Appl. Phys. Lett.* **85**, 902 (2004).
- <sup>8</sup>H. B. Yuen, S. R. Bank, M. A. Wistey, J. S. Harris, Jr, and A. Moto, *J. Appl. Phys.* **96**, 6375 (2004).
- <sup>9</sup>D. Bimberg, M. Sondergeld, and E. Grobe, *Phys. Rev. B* **4**, 3451 (1971).
- <sup>10</sup>I. A. Buyanova, W. M. Chen, G. Pozina, J. P. Bergman, B. Monemar, H. P. Xin, and C. W. Tu, *Appl. Phys. Lett.* **75**, 501 (1999).
- <sup>11</sup>A. Kaschner, T. Luttger, H. Born, A. Hoffman, A. Yu Egorov, and H. Riechert, *Appl. Phys. Lett.* **78**, 1391 (2001).
- <sup>12</sup>M. A. Pinault and E. Tournie, *Appl. Phys. Lett.* **78**, 1562 (2001).
- <sup>13</sup>J. Misiewicz, P. Sitarek, K. Ryczko, R. Kudrawiec, A. Fischer, M. Reinhardt, and A. Forchel, *Microelectron. J.* **34**, 737 (2003).
- <sup>14</sup>M. Oueslati, M. Zouaghi, M. E. Pistol, L. Samuelson, H. G. Grimmeiss, and M. Balkanski, *Phys. Rev. B* **32**, 8220 (1985).